Mechanisms of Cell Regeneration, Development, and Propagation within a Two-Dimensional Multicell Storm

YUH-LANG LIN, ROY L. DEAL, AND MARK S. KULIE

Department of Marine, Earth, and Atmospheric Sciences, North Carolina State University at Raleigh, Raleigh, North Carolina

(Manuscript received 30 September 1996, in final form 19 September 1997)

ABSTRACT

In this study, mechanisms of cell regeneration, development, and propagation within a two-dimensional multicell storm are investigated using a numerical cloud model. The cell regeneration is explained by the advection mechanism. The following processes occur periodically during cell regeneration: (i) Near the edge of the gust front, the gust front updraft is formed by low-level convergence ahead of the gust front near the surface. (ii) The upper portion of the gust front updraft grows by midlevel inflow since the gust front propagates faster than the basic wind. (iii) The growing cell tends to produce and is flanked by strong compensating downdrafts. The upstream downdraft tends to cut off the growing cell from the gust front updraft. It is found that the period of cell regeneration is inversely proportional to the midlevel, strong relative wind speed. This advection mechanism is different from that proposed by Yang and Houze, which views the rearward propagating cell as gravity waves generated by the quasi-steady updraft moving through the ambient flow.

Cell development and propagation within a two-dimensional multicell storm may be described in terms of two distinctive modes: (i) a growing mode and (ii) a propagating mode. When a growing cell reaches its maximum intensity, it splits and then propagates downstream without amplification. The dynamics of cell development and propagation is explained here by critical level argument. For the growing mode there is growth because of a conditionally unstable environment leading to steering level propagation, while for the propagating mode there is no growth because of a more stable environment leading to propagation relative to the flow (i.e., absence of critical level). It is found that the phase relationship between w' and θ' (w' and u') in the growing mode is different from that in the propagating mode and can be explained by the dominance of latent heating in the thermodynamic equation. The propagating mode is dominated by horizontal advection. The propagating mode exhibits gravity wave properties and propagates faster than the growing mode.

1. Introduction

Multicell storms have been studied extensively in the last two decades, both observationally and numerically (e.g., Browning et al. 1976; Thorpe and Miller 1978; Clark 1979; Wilhelmson and Chen 1982; Dudhia et al. 1987; Fovell and Ogura 1989; Fovell and Dailey 1995). A multicell storm is defined as a storm that is composed of several convective cells throughout various stages of its life and may last from several hours to several days. The individual embedded cells are normally short lived and are generated from the quasi-steady updraft cell located over the leading edge of the density current. This quasi-steady updraft is generated by the sustained convergence produced between the propagating density current and the basic environmental wind. Normally, this quasi-steady updraft grows both vertically and horizontally. A new cell then forms downstream (relative to the storm) of the quasi-steady updraft, moves rearward, and further develops. The new cells are generated in a remarkably periodic fashion with a period on the order of 10 min.

In simulating a three-dimensional severe multicell storm, Thorpe and Miller (1978) proposed that the new cell be generated by the convergence produced by the downdraft associated with the previous cell. In their case, no persistent updraft cell exists at the leading edge of the density current. Wilhelmson and Chen (1982) also found that new cell generation occurs about 5 minutes after the most recent cell produces surface precipitation. Therefore, it would appear that new cell generation is somehow related to outflow enhancement due to this downdraft. However, as pointed out by Wilhelmson and Chen, from other simulations the separation speed between old cells and the outflow seems to be a more general controlling factor on the timing of new cell generation, because the development of new cells is more frequent. In other words, precipitation-induced downdrafts then act primarily to sustain the outflow, but their

Corresponding author address: Dr. Yuh-Lang Lin, Department of Marine, Earth, and Atmospheric Sciences, North Carolina State University at Raleigh, Raleigh, NC 27695-8208.
E-mail: yl_lin@ncsu.edu.

timing is not directly related to the timing of new cell formation.

The conventional *cutoff mechanism* suggests that the spreading cold outflow of an old cell enhances convergence, which then triggers the formation of a new cell. Once a new cell forms at the leading edge of the gust front, the supply of moisture and warm air to the older cell is cut off, causing it to dissipate (Wilhelmson and Chen 1982; Droegemeier and Wilhelmson 1985; Fovell and Ogura 1988). Therefore, new cells form at the leading edge of the gust front in a discrete manner (Chalon et al. 1976; Browning 1977). However, from Fovell and Tan's (1996) analysis, the domain maximum vertical velocity, the gust front updraft, and the horizontal pressure gradient across the gust front are correlated and have the same period as the cell regeneration. This may imply that cell regeneration is forced by the oscillation of the gust front, which is accelerated forward by the evaporative cooling associated with the precipitation-induced downdrafts. Even though Fovell and Tan did not explicitly propose this *gust-front pulsation mechanism*. It is important to investigate the possibility of this mechanism.

A horizontal advective scale related to the tendency for cells to drift rearward in the updraft airflow has also been explicitly or implicitly proposed in a number of studies, such as Thorpe and Miller (1978), Thorpe et al. (1982), Wilhelmson and Chen (1982), Fovell and Ogura (1989, hereafter FO89), and Yang and Houze (1995). In particular, FO89 found that the separation speed between the major cell and the gust front (outflow) increases as the storm-relative midlevel inflow (midlevel inflow) increases. This seems to support the idea of an *advection mechanism* of cell regeneration. However, they argued that the cell updrafts are moving within the front-to-rear jet, which consists of air drawn primarily from low levels (especially in the larger shear cases), and it is not entirely clear why such a relationship should be meaningful. Fovell and Tan (1996) also reported that the rearward movement of the established updrafts themselves does not provide a useful prediction of when the next cell would be produced. On the other hand, the low shear cases in FO89's numerical simulations do show significant midlevel inflow due to the large differences between the low-level shear (Δu) and speed of the gust front. In addition, the simulations of Dudhia et al. (1987) have also demonstrated that the winds at midlevels can have an important impact on storm structure and cell motion. Thus, the advection mechanism, which we propose in this paper, remains a viable option for explaining the cell regeneration within a multicell storm. However, a more rigorous investigation is necessary.

In a recent study, Yang and Houze (1995, YH hereafter) proposed that gravity waves can explain the cellular nature of multicell storms. They pointed out that the phase relationships among perturbation pressure, potential temperature, and the u and w wind components in their two-dimensional multicell simulation can be viewed as indicators that multicells are a gravity wave phenomenon. Yang and Houze suggested that new cells are gravity waves forced by the nearly steady low-level, very intense gust front updraft when it moves through the ambient flow, which then break away from the top of the gust front updraft. The cells, which YH call ''gravity-wave updrafts,'' then propagate rearward at their Doppler-shifted gravity wave phase speeds, which increase as the cells near the trailing stratiform region (see their Fig. 16). Based on the scale or wavelength of the cell or the gravity wave, YH argued that the gravity wave speed relative to the storm motion determines the oscillation period of cell regeneration. Yang and Houze offer no explanation for this sudden increase in cell speed, which we see in our simulations as well. In simulating two-dimensional West African multicell squall lines, Dudhia et al. (1987) has also indicated that the periodicity of new cell development may be caused by either a gravity wave response or by microphysical aspects controlling the rate of rain production. Even though YH's argument appears to be reasonable, the following questions remain unanswered: (i) Why does the gravity wave updraft break away from the top of the gust front updraft periodically if the gust front is steady and (ii) why does the downstream gravity wave mode tend to grow, while the upstream mode does not? We will try to examine this *gravity wave mechanism* and answer these questions in this study. In addition, Fovell and Tan (1996) commented that although gravity waves are often excited in the surrounding stable environment by (steady and unsteady) convective motions, their simulated convective cells are not internal gravity waves (which should move rearward faster than the airflow in which they are embedded). In order to support their argument against the gravity wave mechanism of cell regeneration, Fovell and Tan examined the equivalent potential temperature (θ_e) field, which showed that their convective cells move more slowly than the ambient air. Since the gravity waves described by Yang and Houze were produced in a conditionally unstable atmosphere, this implicitly implies that the wave–CISK mechanism (e.g., Lindzen 1974; Raymond 1975, 1976, 1984) may also be at work in the multicell storm. This mechanism needs to be examined.

In a recent study, Fovell and Tan (1996) found that a *convective trigger,* that is, a vapor perturbation zone, may be located upstream of the gust front updraft (GFU), which drifts toward the storm with the speed of the embedded flow. Since the atmosphere is conditionally unstable above the GFU, this vapor pocket may grow in size suddenly when it moves over the GFU.

In section 2, a description of the numerical model and the initial conditions are presented. Then, in section 3, dynamics associated with the simulated cell regeneration from the numerical experiments is discussed. In section 4, the mechanism of cell development and propagation will be described and discussed. Finally, a summary of our findings is presented in section 5.

2. Model description and initial conditions

a. The numerical model

The numerical model employed in this study is the Advanced Regional Prediction System (ARPS) Version 4.0 (Xue et al. 1995), which has been developed at the Center for Analysis and Prediction of Storms (CAPS) at the University of Oklahoma. ARPS is a three-dimensional, compressible, nonhydrostatic cloud model, which is integrated on a staggered, Cartesian grid that can be translated at a time-dependent velocity to keep the major features centered within the computational domain. ARPS has a terrain-following vertical coordinate that may be also stretched to increase the low-level vertical resolution. The model has open lateral boundaries to allow disturbances to exit the computational domain and can be initialized by either a single vertical profile of temperature, moisture, and wind velocity or a three-dimensional observational dataset. The model's sponge layer upper boundary condition is adopted in this study. The Smagorinsky, 1.5-order TKE, and Germano subgrid-scale turbulence schemes are also used. The model utilizes second-order vertical centered differencing and allows the user to choose either second- or fourth-order horizontal centered finite differencing. Leapfrog time differencing is employed and the split-explicit scheme is used to treat the gravity wave and acoustic wave modes. ARPS model microphysics includes both the Kessler warm rain parameterization and the Lin–Farley–Orville (1983) ice microphysics parameterizations, which includes interactions between cloud water, cloud ice, rain, snow, and hail. The prognostic perturbation variables include the u, v, and w wind components; potential temperature; pressure; and the following mixing ratios: water vapor, cloud water, rainwater, cloud ice, snow, and hail. The details of the model can be found in the ARPS User's Guide (Xue et al. 1995).

b. Model input parameters

For the simulation results to be presented in this paper, fourth-order (second-order) finite differencing of the advection terms is used in the horizontal (vertical). The model is run in a two-dimensional mode. The Coriolis force and surface drag are neglected since they play insignificant roles on the short-lived multicell storms. The lower boundary of the domain is flat, rigid, and free slip. The sponge layer is constructed by using a Rayleigh friction, which has a coefficient prescribed by $\nu(z) = (\nu_t/2)\{1 - \cos[\pi(z - z_1)/(z_t - z_1)]\}$ in the sponge layer, where z_1 is the height of the bottom of the sponge layer, z_t the height of the top of the domain, and ν_t the maximum Rayleigh friction coefficient. In this study, we have adopted the following parameters: $z_1 = 12$ km, $z_t = 22$ km, $\nu_t = 0.01$ s^{-1}. The inverse of ν_t is 20 times the large time step (5 s), as recommended by Xue et al. (1995). Note that the small time step is 1 s in this study. The computational domain is two-dimensional with a horizontal resolution of 1 km and a vertical resolution that varies from 200 m at the ground to 800 m at the domain top. The model domain is chosen to be 500 km in the x direction and 22 km in the z direction. The horizontal grid interval in this study is uniform, unlike the horizontally stretched grid adopted by FO89 and Fovell and Dailey (1995). By using a model with a moving grid as well as employing relatively large horizontal domain (500 km) and an Orlanski-type open boundary condition, we are able to minimize wave reflections from the lateral boundaries.

c. Initial conditions

The temperature and moisture profiles used to initialize ARPS are the same as those used by Fovell and Ogura (1988). We choose this sounding because it has been used in previous numerical studies of multicellular convection (Fovell and Ogura 1988, 1989; Fovell and Dailey 1995). Use of this sounding with an improved upper boundary condition will provide us with a more reasonable simulation with respect to buoyancy-driven (i.e., gravity wave) processes and therefore will allow us to determine what role this mechanism plays in the cell regeneration period of multicell storms. The sounding (Fig. 1a) is a *smoothed* version of the HNT (Hinton, Oklahoma) 1430 CST sounding presented by Ogura and Liou (1980) in their case study of a midlatitude squall line that occurred on 22 May 1976. The squall line passed HNT approximately 6.5 h after the sounding was taken. The smoothed sounding's CAPE is roughly 2500 J kg^{-1}. Its lifting condensation level is 1.8 km, and its level of free convection is 2 km. The level of neutral buoyancy is located at $z = 11.2$ km. Note that the environmental lapse rate is nearly dry adiabatic up to 800 mb, so there is no convective inhibition. The vertical profiles of ground-relative wind are shown in Fig. 1b. In each case, the basic wind is westerly and its speed increases linearly with height from zero at the ground up to $z = 2.5$ km. Above 2.5 km, there is no vertical wind shear. Five cases with basic wind speed changes of 7.5, 10, 12.5, 15, and 20 m s^{-1} over the lowest 2.5 km of the model atmosphere are investigated. For later reference, the experiments will be referred to by the change in the basic wind speed from 0 to 2.5 km; for example, $\Delta U = 7.5$ m s^{-1}, 10 m s^{-1}, etc. Convection is initiated in the model by introducing a 2-K warm bubble having a horizontal radius of 5 km and a vertical radius of 1 km. The distribution function in both horizontal and vertical directions are sinusoidal functions. The bubble is placed 100 km from the western boundary of the model domain and is centered at a height of 1 km. The model domain is translated so as to keep the major features in the central portion of the domain.

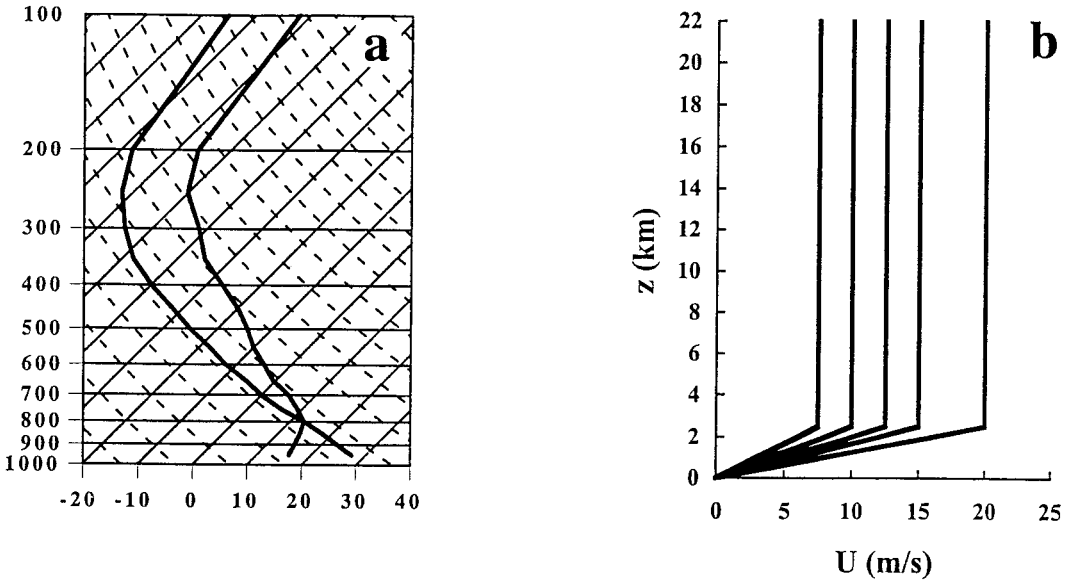

FIG. 1. (a) Skew-*T* plot of the temperature and dewpoint profiles used in the simulations. This is a smoothed version of the 1430 HNT 22 May 1976 sounding presented in Ogura and Liou (1980). (b) Wind profiles used to initialize the simulations.

3. Dynamics of cell regeneration

a. Qualitative summary of storm organization and cell regeneration

After being initialized, all of the modeled storms undergo a period of organization. During this period (typically 60 min), the initial thermal generates a strong updraft that is tilted in the downshear direction. By about 70 min, a sufficient amount of precipitation has evaporated in the dryer subcloud air such that a cold pool forms. The eastern and western sides of the cold pool then begin to propagate downstream (west) and upstream, respectively. A permanent updraft, which is forced by lifting of potentially unstable boundary layer air by the gust front, becomes established along the eastern edge of the outflow. We will refer to this feature as the gust front updraft. Also at this time, cells begin to separate periodically from the GFU and propagate rearward relative to the gust front, and their updrafts begin to tilt upshear. Weaker nonprecipitating convection occurs along the western gust front. Based on results from their three-dimensional modeling study, Rotunno et al. (1988) proposed that convection should be most intense (for a given amount of buoyancy) when the low-level environmental shear is of opposite sign but equal in magnitude to the vorticity produced by buoyancy gradients across the gust front. When this is the case, updrafts in their simulations are more vertically oriented since the positive buoyancy of parcels is aided by vertical acceleration at the gust front. Lin and Chun (1991) obtained a similar result in a two-dimensional modeling study. This appears to be the case for updrafts forming on the eastern edge of the gust front in our simulations since the environmental vorticity is positive, whereas the baroclinic vorticity along the outflow edge is negative. Conversely, the vorticities at the western edge of the gust front are both positive. Hence, one would expect that the boundary layer parcels accelerate as the western edge receives a more horizontal push, resulting in weaker, more slanted convection. This also explains the discrepancy in the formation of convection on opposite sides of the cold pool.

Each simulation in this study is terminated at $t = 6$ h. FO89 found that the convective systems in their simulations typically did not begin to exhibit very steady oscillations until around $t = 5$ h. They defined the beginning of the mature stage as the time when convective cells began to exhibit quasi-steady oscillations (e.g., after $t = 300$ min, their Fig. 6a). We find that the oscillations in our simulation are reasonably steady after $t = 4$ h. Hence the analysis that we present concentrates on the last two hours of model integration.

→

FIG. 2. Vertical cross sections of vertical velocity (thin contours in intervals of 1 m s^{-1}) for a portion of the computational domain in the moving frame of reference with the gust front for the $\Delta U = 10$ m s^{-1} case. Positive (negative) values are solid (dashed). The density current may be roughly represented by the -1 K potential temperature perturbation contour (bold dashed) near the surface. The rainwater is shaded (>0.0005 g kg^{-1}) and the cloud boundary is bold contoured (>0 g kg^{-1}). The corresponding integration time is shown at the top of each panel.

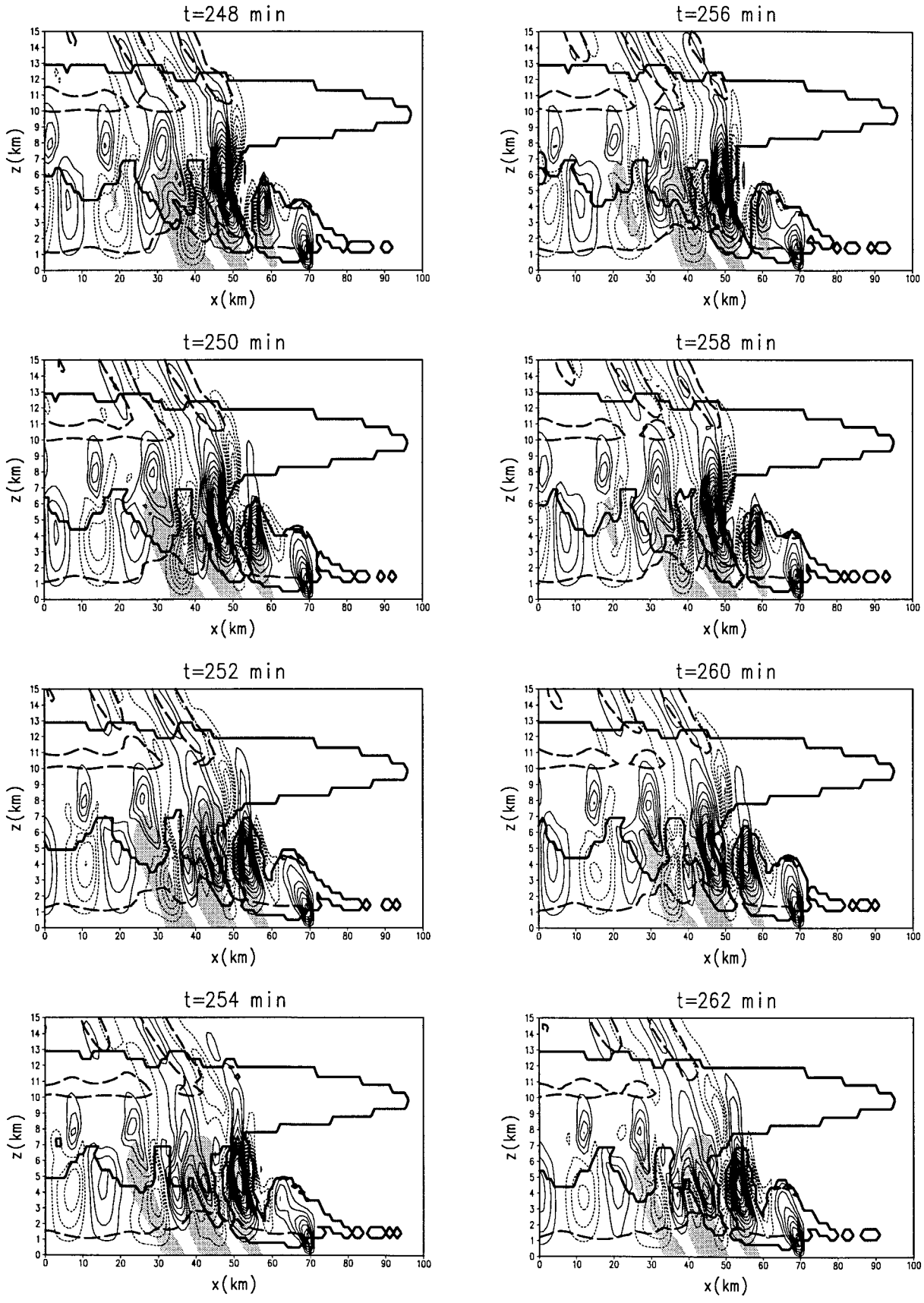
t=248 min
t=256 min
t=250 min
t=258 min
t=252 min
t=260 min
t=254 min
t=262 min
z(km)
x(km)

In all the cases that we perform, cells begin to separate from the GFU at a quasi-steady interval by $t = 4$ h. In the $\Delta U = 7.5$ and 10 m s^{-1} cases, cells form and decay regularly, which is characteristic of the classic multicell. This type of multicell may also be called the strong evolution storm, in contrast to the weak evolution storm defined by Foote and Wade (1982). The weak evolution storm studied by them possesses an updraft that is too unsteady to be considered a squall line. On the other hand, the individual cells are not totally independent from each other, so it cannot be described as a classic multicell. Figure 2 is a series of plots showing a time sequence of the vertical velocity field (w') in the moving frame of reference of the gust front for the $\Delta U = 10$ m s^{-1} case between $t = 248$ and 262 min. Also shown in each panel is the -1 K perturbation potential temperature contour, from which one may discern the outline of the density current and the gust front at low levels. The gust front moves to the east at approximately 17.7 m s^{-1} during this time interval. The corresponding cloud outline as well as the rainwater mixing ratio field are also shown.

Four major updrafts are present at $t = 248$ min between $x = 20$ and 80 km in Fig. 2, including the GFU, which can be found at the density current's leading edge. The other three updrafts represent convective cells in different stages of development with older cells located toward the west. For example, the relatively small updraft at $x = 60$ km is the youngest cell shown. It has just separated from the GFU and has begun to propagate westward relative to the gust front. It is in the process of strengthening and is beginning to form rain within its updraft, which can be seen in the rainwater mixing ratio field (shaded region). The cell at $x = 48$ km has recently reached its peak strength and is producing rainfall at the surface. A relatively heavy concentration of rainwater can be found in its updraft at midlevels. Later on, this suspended precipitation will fall out and produce a significant amount of rainfall at the surface, similar to the current behavior of the cell centered at $x = 35$ km at this time. This cell's updraft has begun to weaken, unloading rainwater at midlevels and producing the heaviest surface rainfall of all the cells. Notice that the rain falls down toward the east, which is responsible for producing the downdrafts at lower levels. At later times, this updraft starts to split at low levels. The splitting process appears to be associated with the mechanism of rainwater loading (e.g., Klemp and Wilhelmson 1978; Thorpe and Miller 1978), as revealed by the rainwater contours (Fig. 2). Almost all of the rain has fallen out of the oldest cell at $x = 20$ km. It has weakened considerably and is producing only very light virga at this time. The cloud associated with this dying cell has eroded at low and midlevels, leaving only a high cloud that has combined with the remnants of previous cells to produce the stratiform region at the rear (i.e., western portion) of the storm.

We can summarize the life cycle of an individual cell for this particular case as follows. First, the GFU begins to expand vertically (e.g., Fig. 2 at $t = 252$ min), signaling the release of a new convective cell, which occurs at an interval of 9.6 min in this particular case. As the new cell moves rearward relative to the gust front, compensating downdrafts begin to form on either side. This aids its separation from the GFU, after which the cell strengthens and begins to precipitate as it moves into the modified air at the rear of the system. The cell begins to split at low levels, which appears to be the results of rainwater loading. Subsequently, another cell develops at the GFU. Due to its supply of less buoyant low-level air being cut off by this new cell, the mature updraft weakens, releases all of the rain that has been collecting in it at midlevels, and then continues to dissipate as it enters the trailing stratiform region. The process then repeats itself, leading to a series of cell growth and decay, characteristic of the strong evolution model, that is, classic multicell storm (Foote and Wade 1982).

b. Roles played by midlevel inflow and low-level front-to-rear inflow in cell regeneration

FO89 and Fovell and Dailey (1995) demonstrated that the periodic behavior of multicell storms can be more complex than that outlined in the traditional multicell model. They found subharmonics in the cell regeneration period (i.e., cells begin to appear in sets of two and then in sets of three) as the low-level shear increases or as the shear layer depth increases. Each set of cells is characterized by a strong cell followed by either one or two weaker cells. Moreover, discrete cell formation gives way to the formation of cells that seem to be less independent of each other, behavior which they concluded to be the two-dimensional analogy of storms undergoing ''weak evolution'' (Foote and Wade 1982). This complex behavior does not become evident until $\sim$5 h in their simulations when the storms settle into a ''quasi-equilibrium'' state. We, too, find this complex behavior in our numerical simulations, although it occurs earlier ($t \sim 4$ h). The shorter organizational period compared to that of FO89 may be in part due to microphysical differences, although it can also be influenced by a wide variety of physical and numerical factors including input sounding characteristics, grid resolution, physical and computational diffusion, storm speed, domain translational speed, etc. Notice that we include ice microphysics in our experiments, while FO89's runs were ice free. We also find that cell formation becomes less discrete as the low-level shear (and hence the winds above 2.5 km) increases, consistent with their findings. We will not attempt to document every subtle difference between our and FO89's simulation results since they are dynamically similar. Our goal is to determine what controls the rate at which new cells are produced.

All of the storms we simulated—whether strongly or weakly evolving—produce cells in a periodic fashion.

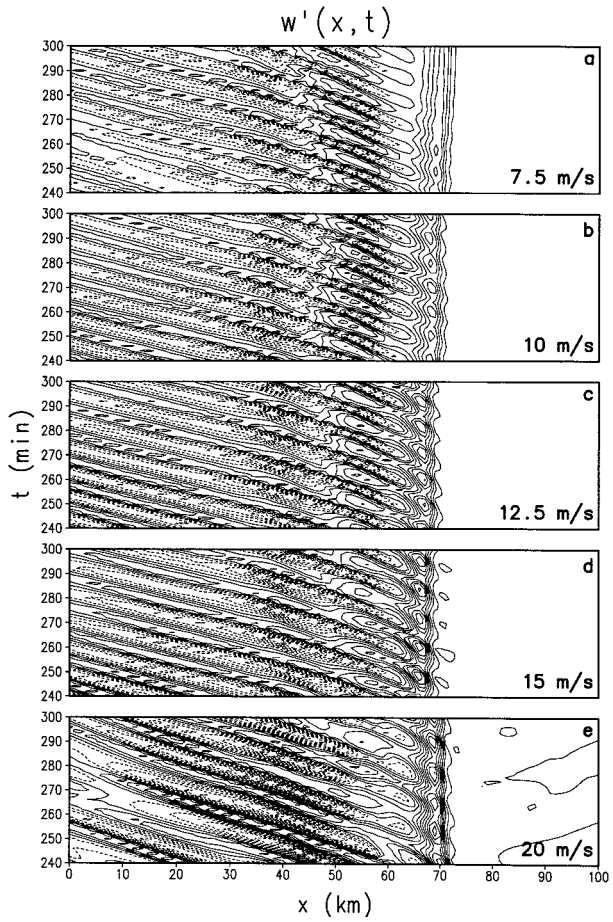

FIG. 3. Time–space plot of vertical velocity at $z = 2.5$ km for the various cases. The base state wind speed at $z = 2.5$ km is given in the upper right-hand corner of each plot. Contour interval is 1 m s^{-1}. Positive (negative) values are solid (dashed). Panels (a)–(e) show cases with $\Delta U = 7.5$, 10, 12.5, 15, and 20 m s^{-1}, respectively.

The regeneration periods are 9.0, 9.6, 10.1, 11.3, and 12.1 min for cases $\Delta U = 7.5$, 10, 12.5, 15, and 20 m s^{-1}, respectively. These estimates are obtained by counting the number of cells that separated from the GFU during the last two hours of model integration from both space–time plots (Fig. 3) and animated of model output on a high performance workstation. The periods are then calculated under the assumption that the cells form at regular intervals. Although this is not strictly the case, it is a very good approximation. Fovell and Dailey (1995) determined the cell periods from a spectral analysis of time series of domain maximum vertical velocity. Of course, a major assumption made in their analysis is that each peak seen in their time series represents the development of a separate cell and, therefore, they are able to follow a single updraft throughout the majority of its lifetime. They also employed two domain-integrated time series, total condensation, and surface rainfall as well, which revealed the same periods and validated the so-called $W_{\max}$ approach. Also, as noted by Fovell and Dailey, the spectrally analyzed periods were checked against animated model results. In fact, the approach used by us, counting cells and averaging, was the technique employed in FO89. Notice that the strength of the GFU oscillates strongly with time, which is consistent with that of Fovell and Tan (1996). This is different from the claim of YH that the GFU is steady. A close inspection of Fig. 3 also indicates that two different rearward propagation speeds of the convective cells exist (see Table 2). As will be discussed later, this implies that there are two different modes of convective cells. The slower (faster) propagation speed of convective cells in the early (later) stages has also been observed (Chalon et al. 1976) and simulated by YH. However, YH offer no explanations for this speed difference when they proposed that cell regeneration and propagation are the manifestation of gravity waves.

One difference between our various simulated storms is the strength of the time-averaged, storm-relative, midlevel inflow (SRMLI). FO89 found that the cells in their simulations move at roughly twice the speed of the midlevel inflow. Thus, it appears that the strength of the midlevel inflow could control the simulated cell speeds. Figure 4 shows vertical profiles of time-averaged, storm-relative inflow for each of the various cases in our study. The profiles are taken 5 km to the east of the gust front, or at $x = 75$ km in Fig. 2, and for the other cases (not shown). The time average is taken using model output at 2-min intervals over the last half (3 h) of the integration. The vertically averaged horizontal wind velocities in the layer from 2.5 to 5.5 km of the various profiles are -12.3, -11.8, -11.1, -9.8, and -8.3 m s^{-1} for cases $\Delta U = 7.5$, 10, 12.5, 15, and 20 m s^{-1}, respectively (see Table 1). This layer is significant because it is the layer in which the newly forming cells are embedded as they begin to separate from the GFU and move rearward. As they move rearward, the cells also propagate upward (at greater slopes with increasing ΔU), eventually attaining depths exceeding that of the 2.5–5.5-km layer, but this generally does not occur until they are well behind the gust front.

The wind velocities far upstream relative to the gust front (SRMLI) are -8.5, -7.7, -7.4, -5.8, and -4.2 m s^{-1} for the cases $\Delta U = 7.5$, 10, 12.5, 15, and 20 m s^{-1} (Table 1). This is also evidenced by the field of vertical velocity superimposed on the equivalent potential temperature field (θ_e) (Fig. 5). Comparing Table 1 to that of FO89, the greater propagation speeds of our simulated storms may be due to ice microphysics that results in and maintains colder, denser cold pools. Notice that θ_e can be considered as a tracer in a moist atmosphere when the air parcel is far removed from a mixing region. Thus, it can be seen clearly from the isentropes in the region ahead (to the right) of the GFU that the newly separated cells are advected rearward by the SRMLI. Therefore, this clarifies the argument proposed by FO89 that the cell updrafts are moving within the front-to-rear jet, which consists of air that is drawn pri-

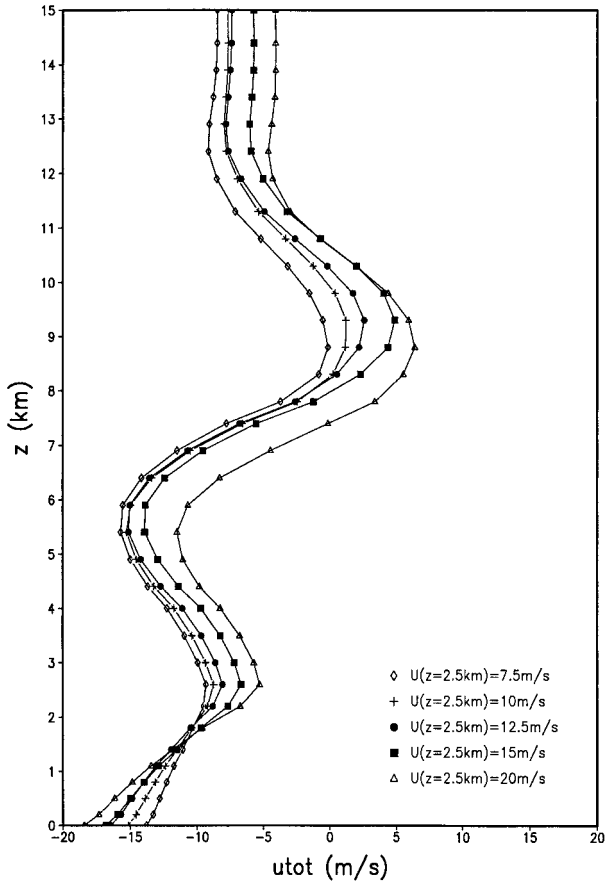

FIG. 4. Vertical profiles of the time-averaged, storm-relative, total u-wind component for each of the five cases. Profile is taken at x = 75 km in Fig. 4, or 5 km to the east of the gust front. The base state wind speed at z = 2.5 km is shown at the top of each panel. The vertically averaged winds in the 2.5–5.5-km layer of the profile are −12.3, −11.8, −11.1, −9.8, and −8.3 m s^{-1} for cases of ΔU = 7.5, 10, 12.5, 15, and 20 m s^{-1}.

marily from low levels. From Fig. 4, one can see that in all cases, the inflow at midlevels ahead of the gust front decreases as the vertical shear of the environmental flow increases. Assuming that the newly separated cells move at the speed of the midlevel inflow, then the period should decrease with increasing midlevel inflow for a constant horizontal cell scale. Figure 6 shows the cell regeneration period versus the far upstream SRMLI (curve a) and the aforementioned 2.5–5.5-km layer-averaged midlevel inflow at x = 75 km (curve b) for the five cases with low-level shear, ΔU = 7.5, 10, 12.5, 15, and 20 m s^{-1}. One can see that the period does decrease (almost linearly) with increasing midlevel inflow, no matter if the far upstream storm-relative or near-storm midlevel inflow speeds are considered. Even though our model integration times are shorter than FO89's, we see results similar to theirs; that is, decreasing midlevel inflow and increasing cell regeneration periods with increasing low-level (0 to 2.5 km) shear. Notice that the midlevel inflow speed increases as ΔU decreases, consistent with the finding of Fovell and Ogura (1988, their Fig. 3b). Thus, *repeating cells* are regenerated by the *midlevel inflow advection* of the growing convective cell from the *upper portion* of the GFU (Figs. 5 and 6), while this growing updraft is *cut off* from the GFU by the *compensating downdraft* associated with it (Fig. 2).

c. A proof of the advection mechanism on cell regeneration

In order to prove the aforementioned *advection mechanism* hypothesized here, we perform a series of experiments with an easterly flow over a plateau with the rainwater deactivated. In this way, the cell is generated by the mountain and the forcing (mountain) is steady state. Therefore, the effects of basic wind advection on new cell generation can be isolated without the complexities induced by the gust front oscillation. By using the same sounding (Fig. 1a), we anticipate that new cells will be generated if the cell generation is independent of the oscillation of the gust front strength. Based on findings from our analysis of Figs. 5 and 6, the cell generation period must be inversely proportional to the midlevel inflow speed if the advection mechanism hypothesis is correct. Also, in the moving frame of the gust front, the far upstream midlevel basic wind speed (SRMLI) decreases as the low-level wind shear (ΔU) increases (see Table 1). For example, the midlevel wind velocity is −8.5 m s^{-1} for case ΔU = 7.5 m s^{-1}, while it is −4.2 m s^{-1} for case ΔU = 20 m s^{-1}. Since we have hypothesized that the advection of cells is due to the midlevel basic wind, we impose a basic wind in the

TABLE 1. Simulated gust front velocities, midlevel inflow velocities, and periods of cell regeneration.

ΔU (m s^{-1})	Gust front velocities relative to ground (m s^{-1})	Midlevel inflow velocities relative to gust front (m s^{-1}) (far upstream SRMLI*)	Layer-averaged (2.5–5.5 km) SRMLI (near gust front)	Period of cell regeneration (s)
7.5	16.0	−8.5	−12.3	9.0
10	17.7	−7.7	−11.8	9.6
12.5	19.9	−7.4	−11.1	10.1
15	20.8	−5.8	−9.8	11.3
20	24.2	−4.2	−8.3	12.1

* SRMLI: Storm relative midlevel inflow.

frame of reference of the gust front (now represented by the mountain), which has a constant surface wind velocity of $U_s = -15$ m s^{-1} that then decreases to -5, -7.5, and -10 m s^{-1} at $z = 2.5$ km and is uniform above this height. Therefore, these cases with midlevel basic wind velocities of $U_{\text{mid}} = -5$, -7.5, and -10 m s^{-1} over the mountain may be considered to correspond roughly to the previous gust front forcing cases with $\Delta U = 20$, 12.5, and 7.5 m s^{-1}, respectively. The constant surface wind also allows us to control the midlevel inflow speed and upslope updraft (corresponding to the gust front updraft in real multicell storm cases), through the linear lower boundary condition $w' = U_s \partial h/\partial x$. The mountain shape is specified by the following analytic function,

$$\begin{aligned} h(x) &= h_0 && \text{for } x \le x_0 \\ h(x) &= h_0 \cos\frac{\pi}{2}\frac{(x - x_0)}{a} && \text{for } x_0 < x \le x_0 + a \\ h(x) &= 0 && \text{for } x_0 + a < x. \end{aligned} \tag{1}$$

In this series of experiments, we have used the following parameters: $h_0 = 1.5$ km, $a = 6$ km, and $x_0 = 100$ km. Convection is produced by steady orographic forcing instead of the instantaneous warm bubble initiation used previously.

Figure 7 shows a time sequence of the w' fields between $t = 60$ min and $t = 120$ min in 4-min intervals for the case where the midlevel basic wind speed is -5 m s^{-1}. It can be seen from the figure that new cells are indeed being generated by the mountain and grow while they are advected rearward (to the left). This cell regeneration process appears to be similar to the case shown in Fig. 2. Above the convective layer, there exist upward propagating gravity waves as evidenced by the upstream (relative to the cell movement) phase tilt. In addition to the rearward (leftward) propagating cells, there also exist forward (rightward) propagating cells, which do not seem to be able to develop. These forward propagating cells appear to be gravity waves generated by the new convective cells as evidenced in w' fields at midlevels (Fig. 7) and in time–space plots of w at $z = 2.5$ km (Fig. 8a). These results are consistent with the finding of Yang and Houze (1995). The cell regeneration process appears to be very regular, as can be seen from the time–space plot of w' at $z = 2.5$ km (Fig. 8a). An estimate from Fig. 8a gives a period of 9.2 min for this case ($U_{\text{mid}} = -5$ m s^{-1}). In order to verify the advection mechanism hypothesis, we ran two other cases with $U_{\text{mid}} = -7.5$ and -10 m s^{-1}. The behavior of the cell generation and development is similar to those shown in Fig. 7 and thus not plotted. Figures 8b and 8c show the time–space plots of w at $z = 2.5$ km for these two cases, respectively. From these two figures, the periods are estimated to be 8.3 min for the case with $U_{\text{mid}} = -7.5$ m s^{-1} and 5.9 min for the case with $U_{\text{mid}} = -10$ m s^{-1}. This result is plotted in Fig. 9. Therefore, the cell regeneration period decreases almost linearly as the midlevel inflow speed increases, as found in the earlier cases with gust front forcing. Similar to our previous simulations with gust front forcing, the cell splits when it reaches its maximum intensity (e.g., 80 min, Fig. 7).

It is worthwhile to mention that the cell splitting process may be produced by gravity waves alone since no precipitation exists in the present case. This may be explained either by the wave–CISK theory of Raymond (1975, 1976) or the forced gravity wave theory of Lin and Smith (1986). However, a more carefully designed experiment is needed to verify this hypothesis. For example, some water loading may still exist in the system, which may play a role in the cell splitting process. The absence of precipitation in these experiments also shows that the periodicity of new cell development is not caused by microphysical aspects controlling the rate of rain production, as proposed by Dudhia et al. (1987). These experiments also disprove the cutoff mechanism, which suggests that the spreading, low-level cold outflow of an old cell enhances convergence, which then triggers the formation of a new cell. Once a new cell forms at the leading edge of the gust front, the supply of moisture and warm air to the older cell is cut off, causing it to dissipate (Wilhelmson and Chen 1982; Droegemeimeier and Wilhelmson 1985; Fovell and Ogura 1988). Therefore, new cells form at the leading edge of the gust front in a discrete manner (Chalon et al. 1976; Browning 1977). Note that ice microphysics is absent in these experiments with a plateau and that the lower boundary is free slip.

In addition to the argument on the period of cell regeneration, the new cell is cut off from the quasi-steady gust front updraft for cases with gust front forcing or the upslope updraft by the strong compensative downdraft associated with the growing new cell. This can be seen from Figs. 2 and 7 at various times. Thus, we may conclude that *cell regeneration* is produced by the *midlevel wind advection* of the growing convective cell from the *gust front updraft* that is cut off by the *compensating downdraft* associated with this new convective cell.

4. Dynamic of cell development and propagation

As discussed in the introduction, YH proposed that new cells are forced to break away from the top of the GFU by the strong, horizontal, rearward-directed, perturbation pressure gradients that develop across the gust front. The cells, which YH call gravity wave updrafts, then propagate rearward at their Doppler shifted gravity wave phase speeds, which increase as the cells approach the trailing stratiform region (see their Fig. 16). Yang and Houze offer no explanation for this sudden increase in cell speed, which we see in our simulations as well. In addition, it remains unclear why the downstream (left) gravity wave mode tends to grow while the gust

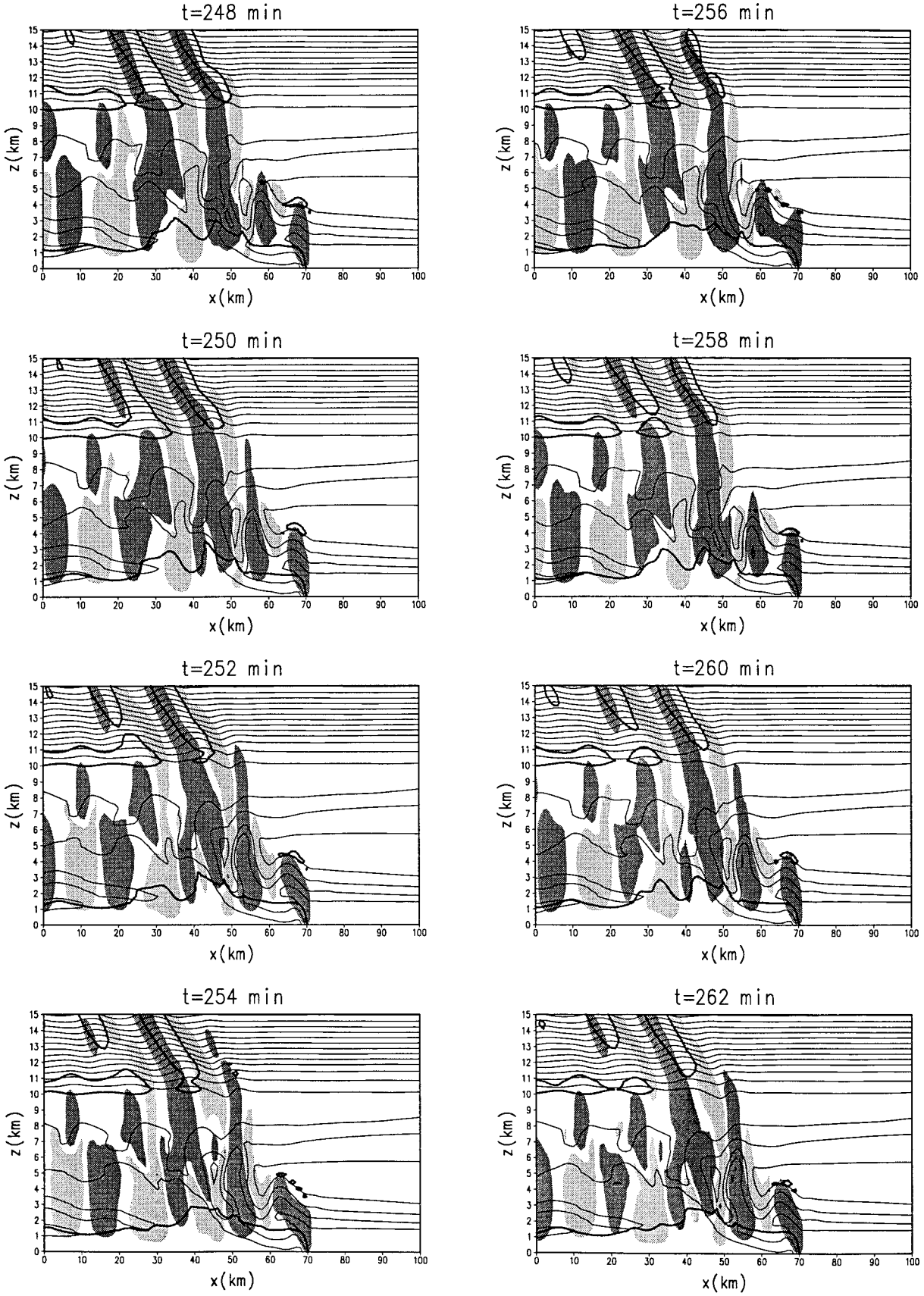
t=248 min
t=256 min
t=250 min
t=258 min
t=252 min
t=260 min
t=254 min
t=262 min
z(km)
x(km)

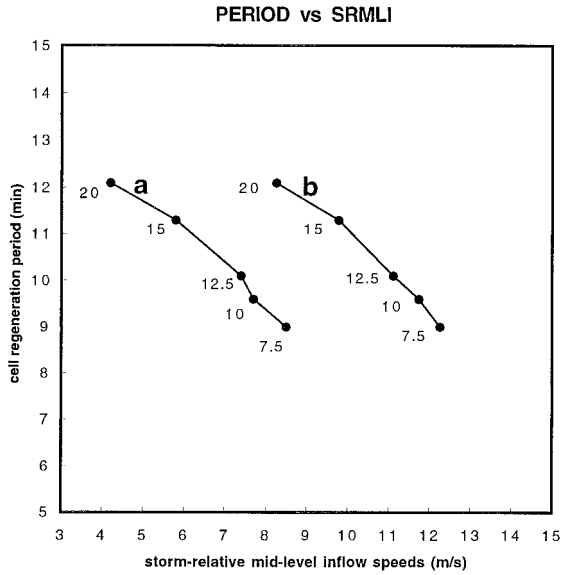

FIG. 6. (a) Cell regeneration period (y axis) vs the far upstream storm relative midlevel inflow (SRMLI) speeds for the profiles shown in Fig. 3 (curve a). The ΔU (in m s^{-1}) is shown beside its corresponding point. (b) Same as (a) except 2.5–5.5-km layer averaged near-storm SRMLI (curve b).

front updraft and the upstream mode do not grow. As discussed in the introduction, since the gravity waves proposed by YH exist in a conditionally unstable atmosphere, this implies that the wave–CISK mechanism may be at work in the multicell storm. In this section, we will examine this mechanism.

Figure 10 shows plots superimposing perturbation pressure (p'), perturbation horizontal velocity (u'), perturbation potential temperature (θ'), and vertical velocity (w') fields at $t = 262$ s. These fields exhibit the following characteristics. (i) The low pressure perturbations are located one-quarter wavelength behind (to the left of) the updrafts in the lower layer ($z' < 4$ km in the present case), one-quarter wavelength ahead of the updraft in the middle layer (4 km $< z <$ 9 km), and are collocated with the downdrafts aloft (9 km $< z$). (ii) The u' maxima are located one-quarter wavelength behind the updrafts in the lower layer and are collocated with the downdrafts in the upper layer. In the middle layer, the u' maxima are located one-quarter wavelength ahead of the updrafts for $x < 40$ km, while they are collocated with the downdrafts for 40 km $< x <$ 70 km. (iii) In both lower and middle layers, the maximum potential temperature perturbations are collocated with the updrafts for 40 km $< x <$ 70 km and are located behind the updrafts for $x < 40$ km. Aloft, the maxima in θ' is located one-quarter wavelength behind the updrafts. These characteristics are the same as those found by YH, except for the phase relationship between θ' and w' in the lower and middle layers and that between u' and w' in the middle layer for 40 km $< x <$ 70 km. A close inspection of YH's Figs. 10 and 12 indicate that although these relationships also existed in their results, they were not clearly recognized. In other words, the phase relationship between w' and θ' (w' and u') is different between the earlier and later stages of cell development. These two stages of cell development can also be detected on the time–space plot of the vertical velocity w' at $z = 2.5$ km (Fig. 3). For $\Delta U = 10$ m s^{-1} (Fig. 3b), it appears that the propagation speeds of the convective cells are slower for $x > 40$ km, while they are faster for $x < 40$ km. In other words, the cell propagation speed is slower in the growing stage and faster in the propagating stage after cell splitting. This also occurs for the cases with orographic forcing (Fig. 8).

This difference in phase relationships between the growing and propagating stages may be explained with the help of the linearized thermodynamic equation governing the two-dimensional small amplitude perturbation in a uniform basic flow (U),

$$\frac{\partial \theta'}{\partial t} + U\frac{\partial \theta'}{\partial x} + \frac{N^2\theta_0}{g}w' = \frac{\theta_0}{c_pT_0}q', \tag{2}$$

where q' is the diabatic heating rate per unit mass and $N^2 = (g/\theta_0)d\bar{\theta}/dz$. Assuming that the latent heat is released when the air is ascending, provided the incoming air is saturated, then the elevated latent heating associated with precipiation may be crudely parameterized by (e.g., Barcilon et al. 1980; Lin 1994a)

$$q' = \frac{c_pT_0N^2}{g}\varepsilon w'\alpha, \tag{3}$$

where

$$\varepsilon = 1 - \frac{N_w^2}{N^2},$$

$$N^2 = \frac{g}{\bar{T}}(\Gamma_d - \Gamma),$$

$$N_w^2 = \frac{g}{\bar{T}}(\Gamma_s - \Gamma),$$

$$\alpha = \begin{cases} 1 & \text{if } w' > 0 \\ 0 & \text{if } w' < 0. \end{cases}$$

In the above, Γ_d and Γ_s are dry and moist lapse rates, respectively; N_w is the moist Brunt–Väisälä frequency.

←

FIG. 5. Vertical cross sections of vertical velocity (dark shaded for $w > 1$ m s^{-1} and light shaded for $w < -1$ m s^{-1}) and equivalent potential temperature fields for a portion of the computational domain in the moving frame of reference with the gust front for the case of $\Delta U = 10$ m s^{-1}. The corresponding integration time is shown at the top of each panel.

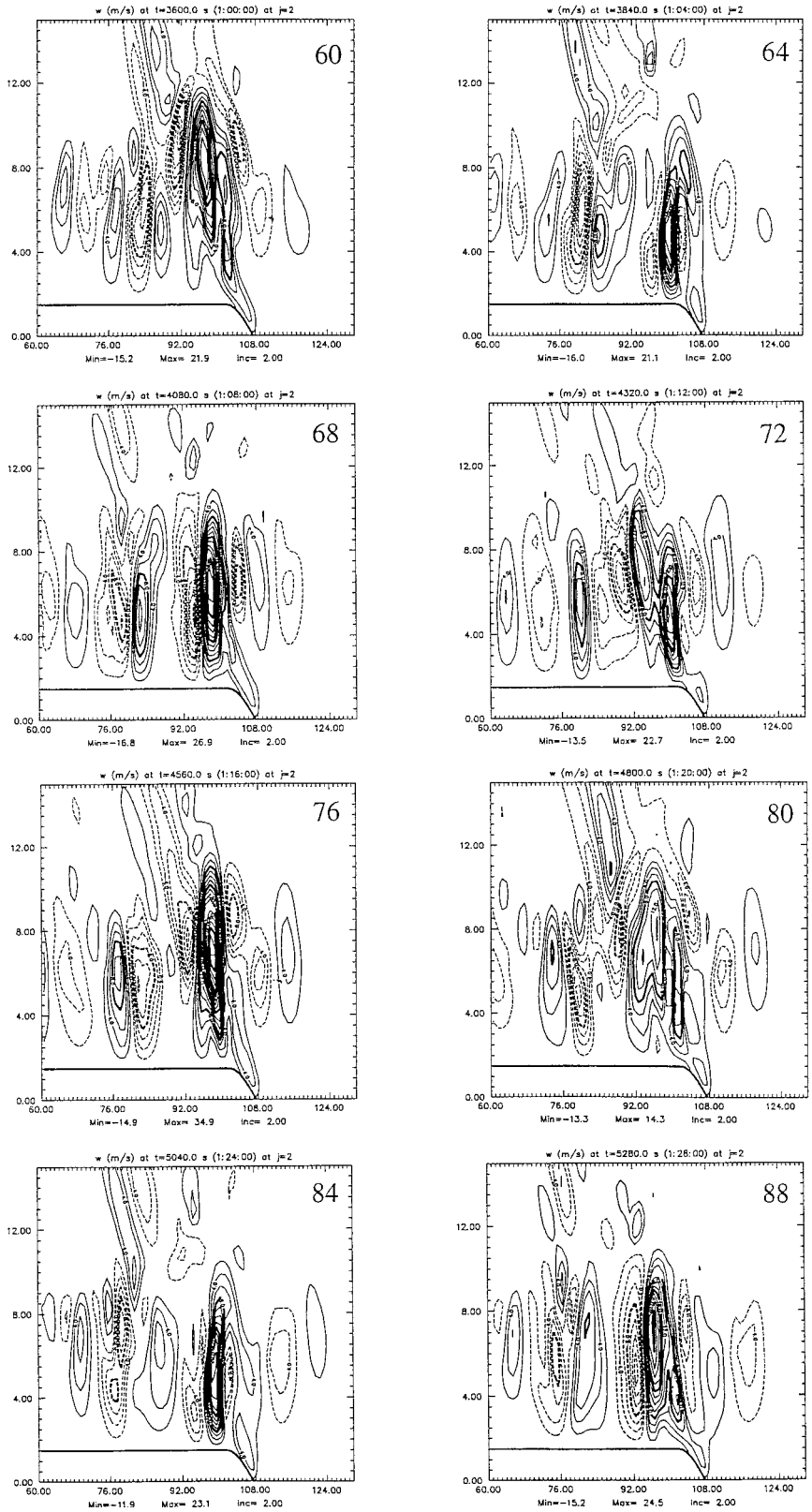

FIG. 7. Vertical cross sections of vertical velocity (contours in intervals of 1 m s^{-1}) fields for an easterly flow over a plateau. The mountain height (h_0) and horizontal scale (a) [Eq. (1)] used are 1.5 and 6 km, respectively. The sounding used is the same as Fig. 1a, while the basic wind

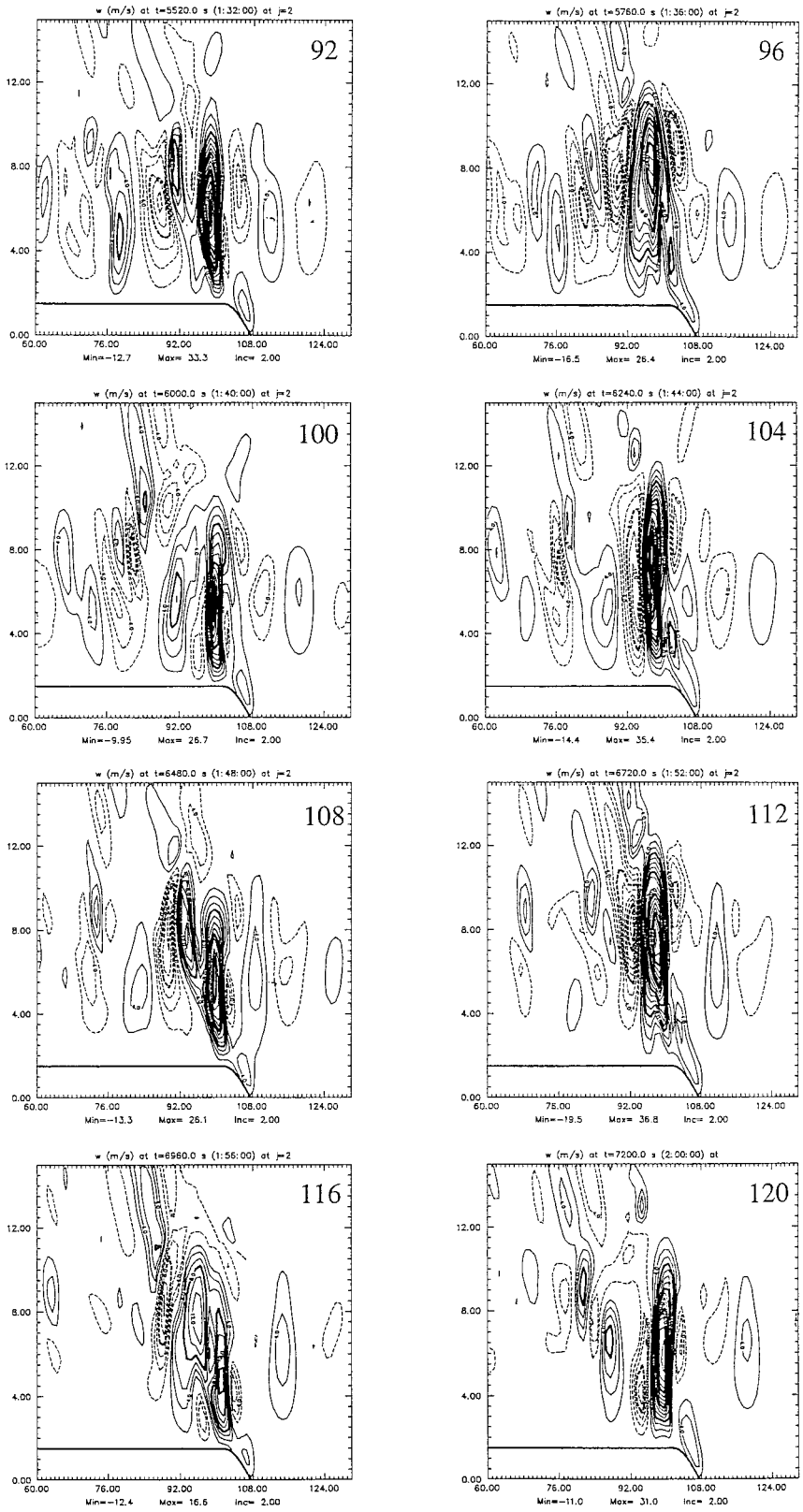

FIG. 7. (*Continued*) profile has a uniform wind velocity of -5 m s^{-1} above 2.5 km and increases linearly to -15 m s^{-1} at surface. The corresponding integration time is shown at the top of each panel.

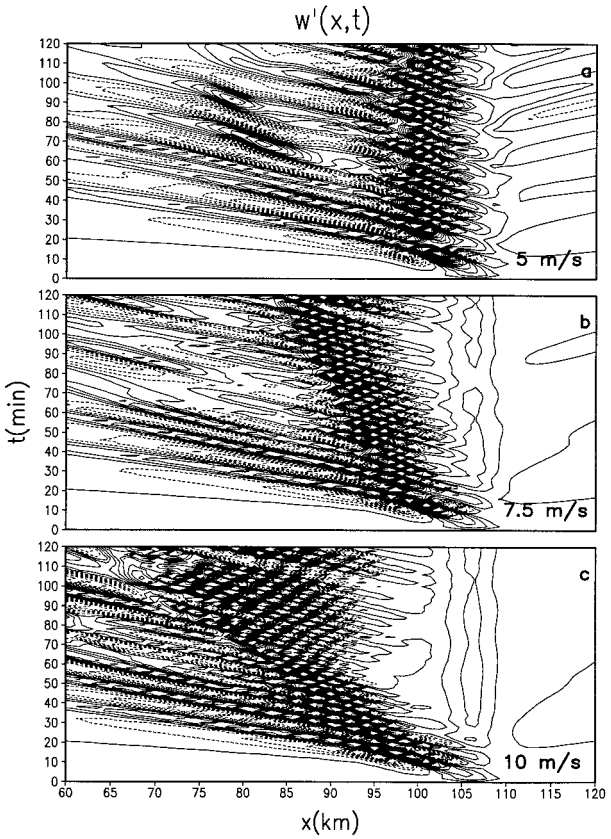

FIG. 8. Time–space plots of vertical velocity at $z = 2.5$ km for three easterly flows over a plateau. The base state wind speed above $z = 2.5$ km is given in the lower right-hand corner of each plot. The contour interval is 1 m s^{-1}. Positive (negative) values are solid (dashed). Panels (a)–(c) show cases with $U_{\text{mid}} = -5$, -7.5, and -10 m s^{-1}, respectively. Notice the surface wind velocity is fixed at -15 m s^{-1} for every case, which decreases linearly with height to a uniform wind velocities of -5, -7.5, and -10 m s^{-1} above 2.5 km.

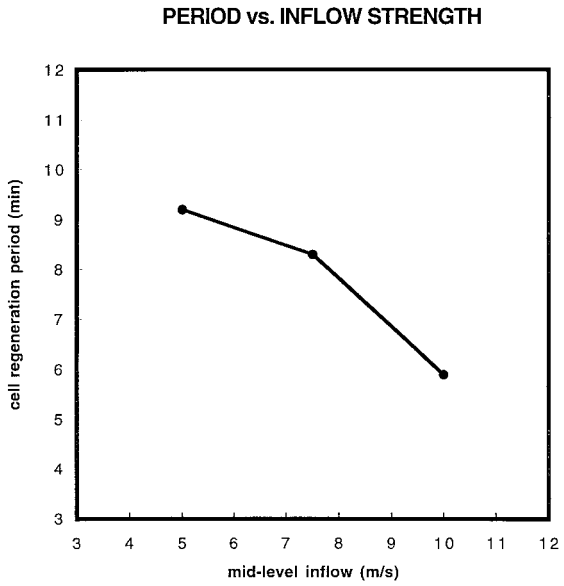

FIG. 9. Cell generation period vs the midlevel inflow speed for flows over a plateau. This figure may be compared with Fig. 6.

In a stable atmosphere, ε is less than 1, while it is greater than 1 in a conditionally unstable atmosphere since $\Gamma_s \leq \Gamma \leq \Gamma_d$ (e.g., Lin 1994a). In the downdraft region, it is assumed that the rain falls out immediately to the ground and thus induces no evaporative cooling. Substituting Eq. (3) into Eq. (2), we obtain

$$\frac{\partial \theta'}{\partial t} = -U\frac{\partial \theta'}{\partial x} - \frac{N^2\theta_0}{g}(1 - \varepsilon\alpha)w'. \qquad (4)$$

During the growing stage of a convective cell, latent heating will make a dominative contribution to the local rate of change of the perturbation potential temperature, compared to the horizontal advection term. As mentioned above, ε is greater than 1 in a conditionally unstable atmosphere, which is true in the present case. Thus, the potential temperature perturbation will be in phase with the w' field, according to Eq. (4). On the other hand, during the propagating stage, a convective cell starts to decay and therefore the latent heating is not as strong as that during the growing stage (see Fig. 11), therefore the horizontal advection term will play more of a role in the local rate of change of perturbation potential temperature. In this way, the maximum potential temperature perturbation will be behind the updraft by one-quarter wavelength, due to the horizontal derivative implied by Eq. (4). In addition, the downstream (leftward) propagation of convective cells is slower during the growing stage since there is more vertical motion.

The dynamics of these two different modes, that is, growing and propagating modes, can be understood from a wave dynamics point of view. Since the gust front moves faster than the basic flow relative to any basic environmental flow far upstream (Table 1), similar to tropical squall lines (Moncrieff and Miller 1976), the wave–CISK mechanism (e.g., Lindzen 1974; Raymond 1975, 1984) appears to be attractive for explaining the maintenance and propagation of the simulated multicell storm presented here. This is because amplifying *forced* linear perturbations can be generated that travel more rapidly than the mean flow at any level (Fernandez and Thorpe 1979; Lilly 1979). In contrast, amplifying *unforced* linear perturbations of a stratified, vertically sheared fluid are constrained by the Miles theorem (Miles 1961) to have a steering or critical level at which the mean flow velocity is equal to the real part of the complex phase velocity. As commented on by Bolton (1980), though the physical mechanisms of buoyancy which are being modeled in these two cases are quite distinct, these two models are rather similar because the diabatic forcing in wave–CISK models is usually chosen to depend on the vertical velocity. Thus, if the diabatic forcing term is actually proportional to the vertical ve-

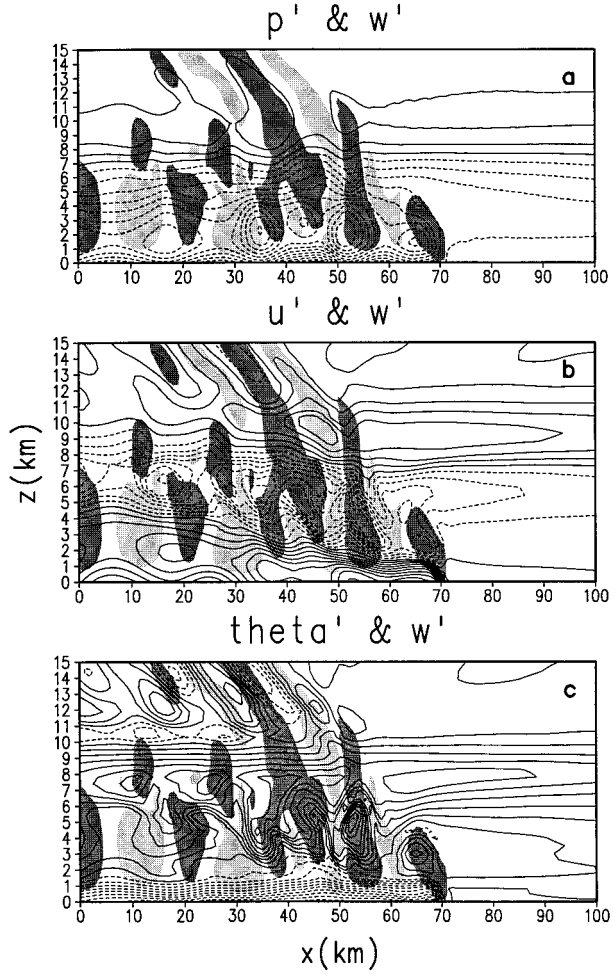

FIG. 10. (a) Perturbation pressure and vertical velocity, (b) perturbation horizontal velocity and vertical velocity, and (c) perturbation potential temperature fields at $t = 262$ s for a portion of the computational domain in the moving frame of reference with the gust front for the case of $\Delta U = 10$ m s^{-1} case. The vertical velocities are dark shaded for $w > 1$ m s^{-1} and light shaded for $w < 1$ m s^{-1}. The density current is roughly represented by the -1 K potential temperature perturbation contour (bold) near the surface. The corresponding integration time is shown at the top of each panel.

locity at each level, then it would reduce to the stratification term of the unforced model.

From Table 1, it can be inferred that no critical levels exist for the entire system moving with the gust front since the gust front is moving faster than the basic wind at every level. However, inspection of the time-averaged, storm-relative, total u-wind component (Fig. 11), and the growing mode speed of the convective cells (second column of Table 2) indicates that critical or steering levels exist for individual cells within the convective system. These critical levels are roughly denoted in Fig. 11. In fact, there are two critical levels for the entire region for cases $\Delta U = 7.5$, 10, and 12.5 m s^{-1} with the critical level heights increasing as one goes rearward (leftward), while they are only present in a relatively narrow region just behind the gust front for cases $\Delta U = 15$ and 20 m s^{-1}. Therefore, the growing mode may be explained within the context of critical level dynamics, which is now presented.

The linear forced Taylor–Goldstein equation for a vertically sheared basic flow can be written (e.g., see Lin 1994a,b)

$$\left(\frac{\partial}{\partial t} + U\frac{\partial}{\partial x}\right)^2 (w'_{xx} + w'_{zz}) - \left(\frac{\partial}{\partial t} + U\frac{\partial}{\partial x}\right) U_{zz} w'_x + N^2 w'_{xx} = \frac{g}{c_p T_0} q'_{xx}. \tag{5}$$

Assuming a wavelike solution, $w = \hat{w}\exp[ik(x - ct)]$, the above equation may be transformed into wavenumber space,

$$\frac{d^2\hat{w}}{dz^2} - \left(k^2 - \frac{N^2}{(U-c)^2} + \frac{U_{zz}}{U-c}\right)\hat{w} = \frac{g\hat{q}}{c_p T_0 (U-c)^2}. \tag{6}$$

Following Miles (1961), let

$$\hat{w} = \frac{D\eta}{Dt} \quad \text{or} \quad w = ik(U-c)\eta. \tag{7}$$

After substituting Eq. (7) into Eq. (6) and imposing the boundary conditions, $\eta = 0$ at z_1 and z_2, we obtain

$$\frac{d}{dz}\left[(U-c)^2\frac{d\eta}{dz}\right] - [k^2(U-c)^2 - N^2]\eta = \frac{-iQ}{k(U-c)}, \tag{8}$$

where

$$Q = \frac{g\hat{q}}{c_p T_0}.$$

Multiplying Eq. (8) by its complex conjugate η^*, integrating from the lower to upper boundary, and then taking the imaginary part yields

$$2\int_{z_1}^{z_2} c_i(U-c_r)\left(\left|\frac{d\eta}{dz}\right|^2 + k^2|\eta|^2\right) dz = \mathrm{Im}\int_{z_1}^{z_2} \frac{-iQ\eta^*}{k(U-c)}\, dz, \tag{9}$$

where $c = c_r + ic_i$ and Im denotes the imaginary part. Following Bolton (1980), we assume the phase of the diabatic forcing Q differs from that of the vertical velocity w' by an amount β,

$$Q = Fe^{i\beta}w', \tag{10}$$

where F and β are real and may vary with height z. The right side of (9) then becomes

$$\int_{z_1}^{z_2} g|\eta|^2 F \sin\beta\, dz. \tag{11}$$

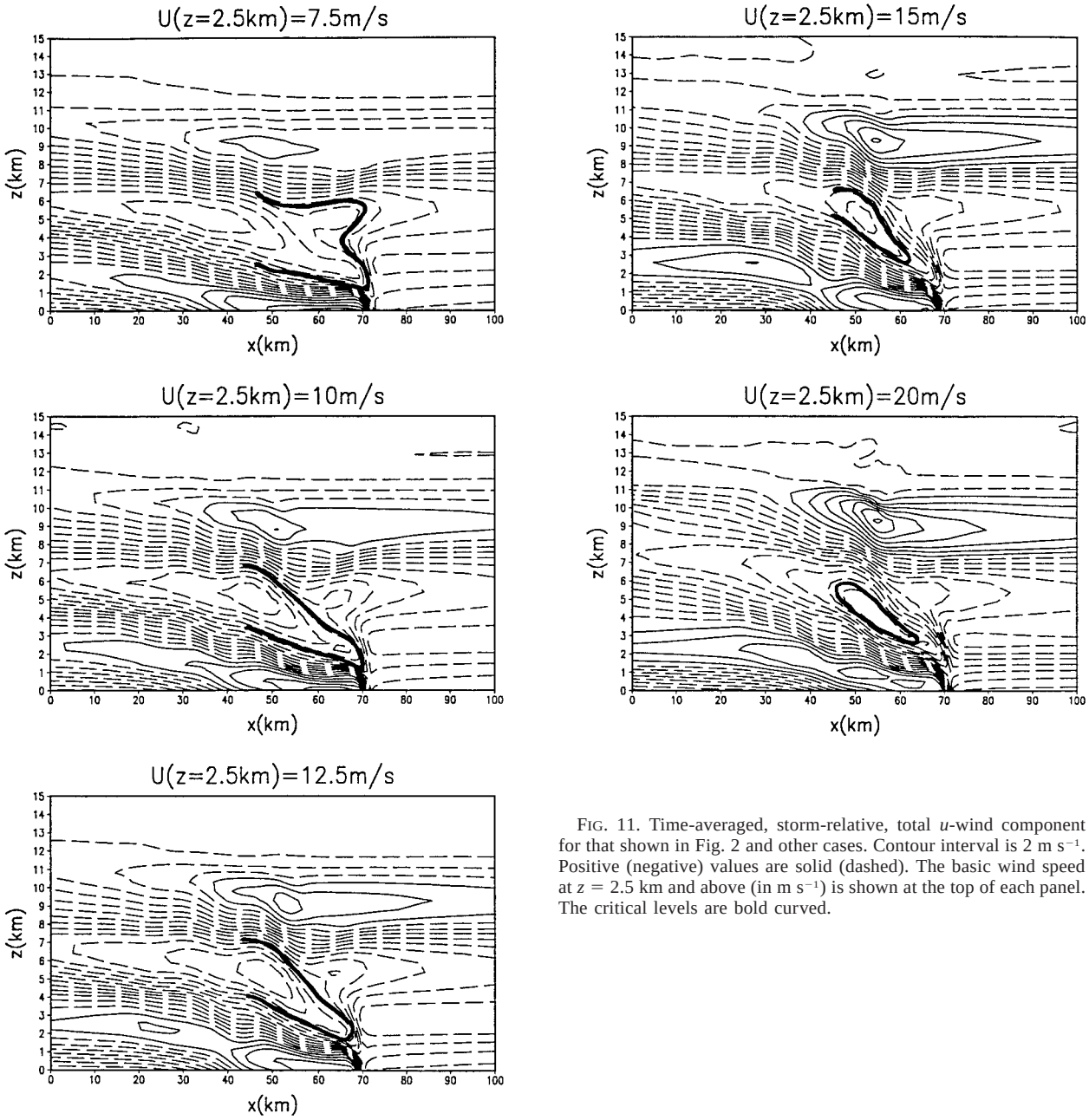

FIG. 11. Time-averaged, storm-relative, total u-wind component for that shown in Fig. 2 and other cases. Contour interval is 2 m s^{-1}. Positive (negative) values are solid (dashed). The basic wind speed at $z = 2.5$ km and above (in m s^{-1}) is shown at the top of each panel. The critical levels are bold curved.

TABLE 2. Simulated speeds of growing mode and propagation mode relative to the gust front.

ΔU (m s^{-1})	Growing mode speed (m s^{-1})	Propagating mode speed (m s^{-1})
7.5	17.3	30.0
10	18.9	29.6
12.5	19.2	32.9
15	22.7	28.0
20	23	24.3

If $\beta = 0$, then (11) equals 0, which in turn indicates that the right-hand side of (9) vanishes. Therefore this implies either $c_i = 0$ or $c_i \neq 0$ and $U - c_r = 0$ somewhere. In other words, if the *diabatic forcing* is in phase with w' everywhere, then either there exists no amplification or if amplification exists, then so must a *steering* or *critical level.* Additionally, Bolton's theorem (Bolton 1980) also states, ''For diabatic forcing to generate an amplifying, non-steering level perturbation, it is necessary that the forcing should be somewhere out of phase with w', as suggested by Moncrieff (1978).''

Figure 12 indicates that the diabatic forcing is almost

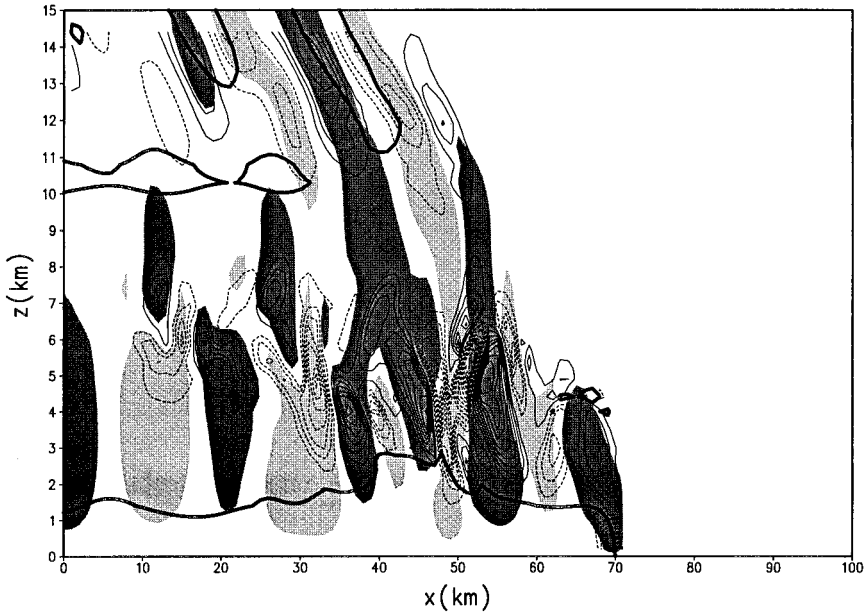

FIG. 12. Heating rates and vertical velocity fields at $t = 262$ s for the case of $\Delta U = 10$ m s^{-1}. The -1 K potential temperature perturbation contours are plotted by bold curves, which denotes the density current near the surface. The vertical velocity fields are shaded as in Fig. 5.

in phase with w' (i.e., $\beta = 0$) for $x < 40$ km in the cloud layer for case $\Delta U = 10$ m s^{-1}. This is also consistent with YH's simulation results but not with their analysis. Notice that this phase relationship is maintained for most of the simulation time except in the upper part at the very early stage of the cell development, which is advected by the midlevel inflow. As mentioned earlier, steering or critical levels also exist in the middle layer during the earlier stage of individual cell development. For example, two critical levels exist for 40 km $< x <$ 70 km for the case with $\Delta U = 10$ m s^{-1} (Fig. 11). Therefore, for the *growing mode*, there is growth because of a *conditionally unstable environment* leading to *steering level propagation.* On the other hand, during the later stage of cell development, the *convective cells* move into a more *stable environment*. Thus, these convective cells cannot grow, leading to *propagation relative to the flow* (i.e., no critical level). For example, the convective cells located to the left of $x = 40$ km for case $\Delta U = 10$ m s^{-1} move rearward (leftward) at a speed of 29.6 m s^{-1}, which is faster than the environmental wind speed at any level (Fig. 11). Therefore, according to the above argument, there is no amplification and the disturbance tends to propagate downstream. In addition, this also explains the vertical development of the upper portion of the gust front updraft, which is then advected by the mean midlevel flow and subsequently becomes the new cell. The forward (rightward) propagating gravity waves cannot develop further because they cannot produce enough lifting.

In a conventional wave–CISK model, even for nonsheared mean flows, the lines of maximum w' normally slope with height, as remarked by Lilly (1979). For Q proportional to w' or dw'/dz at some given level (such as the level of free convection) and then distributed uniformly in the heating layer (as is normally assumed), the lines of maximum forcing, however, will not slope with height (Bolton 1980). This does not seem to be consistent with the present results (Fig. 12). Therefore, the wave–CISK mechanism may not explain the development and maintenance of convective cells within a multicell thunderstorm. Although cell propagation and development does possess gravity wave properties as found by YH, the dynamics are more appropriately explained in terms of the above *critical level argument.* Notice that YH did not discuss the importance of critical levels.

In addition, YH used a linear theory to explain the multicellular structure in the cloud layer of a multicell system as vertically trapped tropospheric gravity waves since the phase line of a trapped gravity wave tends to be vertical (i.e., not tilted with height). On the other hand, it is well known from linear theory that both upward and downward propagating terms must exist in the layer with diabatic forcing (e.g., Smith and Lin 1982; Lin and Smith 1986). Therefore, the phase lines will naturally be vertical. Yang and Houze also suggested that the trapping mechanism responsible for convective systems is similar to orographically forced gravity waves. However, our experiments of conditionally unstable flow over a plateau do not seem to support this trapping mechanism. This can be seen from the presence of rapidly decaying cells farther downstream (to the

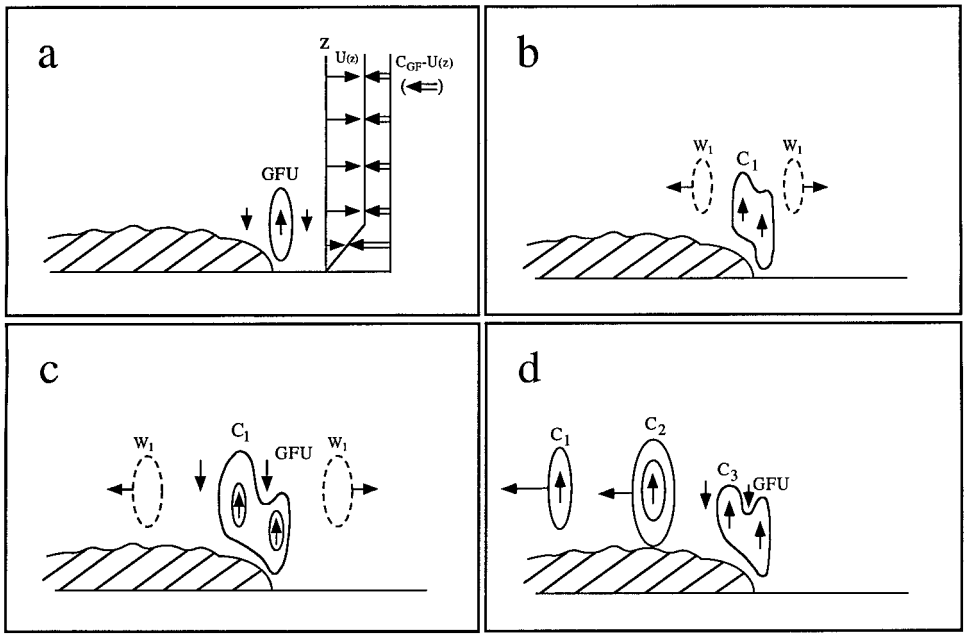

FIG. 13. A schematic model for the cell regeneration and propagation within a two-dimensional multicell thunderstorm. Four stages are found: (a) formation and maintenance of the gust front updraft (GFU), (b) rearward advection of the growing gust front updraft, (c) cutting off of the growing cell (c_1) from the gust front updraft by the upstream compensating downdraft, and (d) cell regeneration and coexistence of the growing (c_2 and c_3) and propagating (c_1) modes.

left), as shown in Fig. 7. Further investigation is needed to clarify this phenomenon.

5. Conclusions and discussion

In this study, mechanisms of cell regeneration, development, and propagation within a two-dimensional multicell storm are investigated using a numerical cloud model. Cell regeneration from the updraft located at the leading edge of the gust front is often observed in nature and simulated by cloud models.

In this paper, cell regeneration is explained by an advection mechanism. The following processes are repeated for cell regeneration (Fig. 13). (i) Near the edge of the gust front, the gust front updraft is formed by the low-level convergence ahead of the gust front near the surface. Weak gravity waves may be generated by this gust front updraft, although they are too weak to be detected in the real atmosphere. (ii) The upper portion of the gust front updraft grows by the midlevel inflow since the gust front propagates faster than the basic wind. Relatively stronger gravity waves are produced by this growing cell (C_1), which is still attached to the gust front updraft. (iii) The growing cell (C_1) tends to produce strong compensating downdrafts on both sides. The upstream (right) downdraft tends to cut off the growing cell from the gust front updraft. During this stage, maxima perturbation potential temperature are collocated with the updrafts in the middle and lower layers. The convective cell-induced gravity waves propagate both upstream and downstream without amplification. This process is verified by analyzing the time evolution of the vertical motion field from the cloud model results and by performing experiments with a basic flow over a plateau. It is found that the period of cell regeneration is inversely proportional to the midlevel, storm-relative wind speed. This advection mechanism is different from that proposed by YH, which views the rearward propagating cell as a gravity wave generated by the propagation of a quasi-steady updraft moving through the ambient flow.

The cell development and propagation within a multicell storm can be described in terms of two distinctive modes: (i) a growing mode and (ii) a propagating mode. When a growing cell reaches its maximum intensity, it splits and then propagates downstream without amplification. The dynamics of cell development and propagation is explained in terms of a critical level argument. For the growing mode there is growth because of a conditionally unstable environment leading to steering level propagation, while for the propagating mode there is no growth because a more stable environment leading to propagation relative to the flow (i.e., no critical level) is present.

For both modes, p', u', θ', and w' fields exhibit the following characteristics. (i) The low-level pressure perturbations are located one-quarter wavelength behind the updrafts in the lower layer, one-quarter wavelength ahead of the updrafts in the cloud layer, and are colocated with the downdrafts in the higher layer. (ii) The

u' maxima are located one-quarter wavelength behind the updrafts in the lower layer and colocated with the downdrafts in the upper layer. In the middle layer, the u' maxima are located one-quarter wavelength ahead of the updrafts for $x < 40$ km (propagating mode), while they are collocated with the downdrafts for 40 km $< x < 70$ km (growing mode). (iii) In both the lower and middle layers, θ' maxima are collocated with the updrafts of the growing mode and are located behind the updrafts of the propagating mode. In the upper layer, the θ' maxima are located one-quarter wavelength behind the updrafts. These characteristics are the same as those found by YH except for the phase relationship between w' and θ' (u') in the lower and cloud layers (cloud layer) during the early stage (growing mode). In other words, the phase relationship between w' and θ' (w' and u') in the growing mode is different from that in the propagating mode. The phase relationship of w' and θ' is explained by the dominance of the latent heating by applying the thermodynamic equation to an analysis of the growing mode. The propagating mode is dominated by the horizontal advection. The propagating mode exhibits gravity wave properties and propagates faster than the growing mode.

It is found that the vertical velocity is oriented vertically and collocated with the maximum thermal forcing for both the growing and propagating modes. However, it appears that the development and propagation of convective cells within a multicell storm may not be supported by conventional wave–CISK theory. Based on the experiment of conditionally unstable flow over a plateau, it is argued that the vertical phase orientation of the vertical velocity may be explained by a forced gravity wave mechanism instead of the trapping mechanism as proposed by YH. A more rigorous study is needed to verify this hypothesis. In order to prove the advection mechanisms, we have used a rigid obstacle to resemble the cold pool. Although we have obtained a significant physical insight of the dynamics by taking this approach, readers are reminded that there exist some differences between the real cold pool and the obstacle proxy, such as 1) no mixing is permitted across the obstacle boundary, 2) the real cold pool has air moving within it, and 3) no baroclinicity generated vorticity created at the obstacle nose.

Acknowledgments. This work is supported by NSF Grant ATM-9224595 and NOAA Grant NA57RA0482. The permission from Dr. K. K. Droegemeier for using the ARPS model and the help from Dr. M. Xue on ARPS are highly appreciated. The authors would also like to thank Dr. C. S. Chen at the National Central University of Taiwan and Dr. M. L. Kaplan at NCSU for valuable discussions, and Dr. R. P. Weglarz at NCSU for proofreading the manuscript. Comments from Dr. R. G. Fovell at UCLA and anonymous reviewers on the original manuscript have improved the quality of this paper significantly. Part of the computations were performed on the CRAY C90 at the North Carolina Supercomputing Center and on the FOAM^{v} workstations at NCSU, which are funded by IBM.

REFERENCES

Barcilon, A., J. C. Jusem, and S. Blumsack, 1980: Pseudo-adiabatic flow over a two-dimensional ridge. *Geophys. Astrophys. Fluid Dyn.,* **16,** 19–33.

Bolton, D., 1980: Application of the Miles theorem to forced linear perturbations. *J. Atmos. Sci.,* **37,** 1639–1642.

Browning, K. A., 1977: The structure and mechanisms of hailstorms. *Hail: A Review of Hail Science and Hail Suppression, Meteor. Monogr.,* No. 38, Amer. Meteor. Soc., 1–43.

——, J. C. Fankhauser, J.-P. Chalon, P. J. Eccles, R. G. Strauch, F. H. Merrem, D. J. Musil, E. L. May, and W. R. Sand, 1976: Structure of an evolving hailstorm. Part V: Synthesis and implication for hail growth and hail suppression. *Mon. Wea. Rev.,* **104,** 603–610.

Chalon, J.-P., J. C. Fankhauser, and P. J. Eccles, 1976: Structure of an evolving hailstorm. Part I: General characteristics and cellular structure. *Mon. Wea. Rev.,* **104,** 564–575.

Clark, T. L., 1979: Numerical simulations with a three-dimensional cloud model: Lateral boundary condition experiments and multicellular severe storm simulations. *J. Atmos. Sci.,* **36,** 2191–2215.

Droegemeier, K. K., and R. B. Wilhelmson, 1985: Three-dimensional numerical modeling of convection produced by interacting thunderstorm outflow. Part I: Control simulation and low-level moisture variations. *J. Atmos. Sci.,* **42,** 2381–2403.

Dudhia, J., M. W. Moncrieff, and D. W. K. So, 1987: The two-dimensional dynamics of West Africa squall lines. *Quart. J. Roy. Meteor. Soc.,* **113,** 121–146.

Fernandez, W., and A. J. Thorpe, 1979: An evaluation of theories of storm motion using observations of tropical convective systems. *Mon. Wea. Rev.,* **107,** 1306–1319.

Foote, G. B., and C. G. Wade, 1982: Case study of a hailstorm in Colorado. Part I: Radar echo structure and evolution. *J. Atmos. Sci.,* **39,** 2828–2846.

Fovell, R. G., and Y. Ogura, 1988: Numerical simulation of a midlatitude squall line in two dimensions. *J. Atmos. Sci.,* **45,** 3846–3879.

——, and ——, 1989: Effect of vertical wind shear on numerically simulated multicell storm structure. *J. Atmos. Sci.,* **46,** 3144–3176.

——, and P. S. Dailey, 1995: The temporal behavior of numerically simulated multicell-type storms. Part I: Modes of behavior. *J. Atmos. Sci.,* **52,** 2073–2095.

——, and P.-H. Tan, 1996: Why multicell storms oscillate. Preprints, *18th Conf. Severe Local Storms,* San Francisco, CA, Amer. Meteor. Soc., 186–189.

Klemp, J. B., and R. B. Wihelmson, 1978: The simulation of three-dimensional convective-storm dynamics. *J. Atmos. Sci.,* **35,** 1070–1096.

Lilly, D. K., 1979: The dynamical structure and evolution of thunderstorms and squall lines. *Annu. Rev. Earth Planet. Sci.,* **7,** 117–161.

Lin, Y.-L., 1994a: Airflow over mesoscale heat sources. Part I: Responses in a uniform flow. *Proc. Natl. Sci. Council,* A18, 1–32. [Available from Dr. Y.-L. Lin, Dept. of Marine, Earth, and Atmospheric Sciences, North Carolina State University, Raleigh, NC 27695.]

——, 1994b: Airflow over mesoscale heat sources. Part II: Responses in a shear flow. *Proc. Natl. Sci. Council,* A18, 119–150. [Available from Dr. Y.-L. Lin, Dept. of Marine, Earth, and Atmospheric Sciences, North Carolina State University, Raleigh, NC 27695.]

——, and R. B. Smith, 1986: Transient dynamics of airflow near local heat source. *J. Atmos. Sci.,* **43,** 40–49.

——, and H.-Y. Chun, 1991: Effects of diabatic cooling in a shear flow with a critical level. *J. Atmos. Sci.,* **48,** 2476–2491.

——, R. D. Farley, and H. D. Orville, 1983: Bulk parameterization of the snow field in a cloud model. *J. Climate Appl. Meteor.,* **22,** 1065–1092.

Lindzen, R. S., 1974: Wave–CISK in the tropics. *J. Atmos. Sci.,* **31,** 156–179.

Miles, J. W., 1961: On the stability of heterogeneous shear flows. *J. Fluid Mech.,* **10,** 496–508.

Moncrieff, M. W., 1978: The dynamical structure of two-dimensional steady overturning in constant vertical shear. *Quart. J. Roy. Meteor. Soc.,* **104,** 543–567.

——, and M. J. Miller, 1976: The dynamics and simulation of tropical cumulonimbus and squall lines. *Quart. J. Roy. Meteor. Soc.,* **102,** 373–394.

Ogura, Y., and M.-T. Liou, 1980: The structure of a midlatitude squall line: A case study. *J. Atmos. Sci.,* **37,** 553–567.

Raymond, D. J., 1975: A model for predicting the movement of continuously propagating convective storms. *J. Atmos. Sci.,* **32,** 1308–1317.

——, 1976: Wave–CISK and convective mesosystems. *J. Atmos. Sci.,* **33,** 2392–2398.

——, 1984: A wave–CISK model of squall lines. *J. Atmos. Sci.,* **41,** 1946–1958.

Rotunno, R., J. B. Klemp, and M. L. Weisman, 1988: A theory for strong, long-lived squall lines. *J. Atmos. Sci.,* **45,** 463–485.

Smith, R. B., and Y.-L. Lin, 1982: The addition of heat to a stratified airstream with application to the dynamics of orographic rain. *Quart. J. Roy. Meteor. Soc.,* **108,** 353–378.

Thorpe, A. J., and M. J. Miller, 1978: Numerical simulations showing the role of the downdraft in cumulonimbus motion and splitting. *Quart. J. Roy. Meteor. Soc.,* **104,** 873–893.

——, ——, and M. W. Moncrief, 1982: Two-dimensional convection in nonconstant shear: a model of mid-latitude squall lines. *Quart. J. Roy. Meteor. Soc.,* **108,** 739–762.

Wilhelmson, R. B., and C.-S. Chen, 1982: A simulation of the development of successive cells along a cold outflow boundary. *J. Atmos. Sci.,* **39,** 1466–1483.

Xue, M., K. K. Droegemeier, V. Wong, A. Shapiro, and K. Brewster, 1995: Advanced Regional Prediction System version 4.0 users guide. CAPS, 380 pp. [Available from ARPS Model Development Group, CAPS, University of Oklahoma, 100 East Boyd, Norman, OK 73019-0628.]

Yang, M.-J., and R. A. Houze Jr., 1995: Multicell squall line structure as a manifestation of vertically trapped gravity waves. *Mon. Wea. Rev.,* **123,** 641–660.